

# Sulfur-doped carbon dots derived from caffeine: A highly efficient photocatalyst for organic dye degradation

Ganyaporn WONGWAEN<sup>1</sup>, Koranat DECHSRI<sup>2</sup>, Praneet OPANASOPIT<sup>2</sup>, Montri AIEMPANAKIT<sup>3</sup>, and Cheewita SUWANCHAWALIT1,\*

#### Received date:

11 March 2025

#### Revised date:

4 June 2025

## Accepted date:

26 August 2025

#### **Keywords:**

Carbon dots;

Caffeine;

Solvothermal:

Photocatalysts;

Sulfur-doped carbon dots

## Abstract

Sulfur-doped carbon dots (S-doped CDs) were synthesized via a solvothermal method using caffeine as a carbon precursor and sodium sulfide as a sulfur source. Characterization using transmission electron microscopy (TEM), X-ray photoelectron spectroscopy (XPS), Fourier-transform infrared spectroscopy (FT-IR), ultraviolet -visible (UV-Vis) spectroscopy, and photoluminescence spectroscopy (PL) confirmed successful sulfur incorporation. TEM revealed a uniform size distribution and graphitic structures, while UV-Vis analysis showed a reduction in the bandgap from 3.29 eV to 3.10 eV, improving light absorption and charge carrier separation. The photocatalytic activity of S-doped CDs was evaluated for indigo carmine (IC) dye degradation under UV irradiation, where 2S-CDs exhibited the highest degradation efficiency (~90% within 240 min) due to enhanced charge carrier separation, defect-state-mediated electron transfer, and the generation of reactive oxygen species (ROS). Radical scavenger experiments confirmed that superoxide radicals (\*O2-), hydroxyl radicals (\*OH), and photogenerated holes (h+) played key roles in dye degradation. This study demonstrates that S-doped CDs derived from caffeine are efficient and sustainable photocatalysts for wastewater treatment.

# 1. Introduction

Water pollution caused by synthetic dyes has become a significant environmental concern due to their extensive use in the textile, printing, and pharmaceutical industries. These dyes are highly stable, nonbiodegradable, and resistant to conventional wastewater treatment methods, posing risks to aquatic ecosystems and human health [2]. Traditional treatment approaches, including coagulation, adsorption, and chemical oxidation, are often insufficient for complete dye removal, necessitating the development of efficient and sustainable alternatives [3]. Among advanced treatment technologies, photocatalysis has emerged as a promising green approach, offering the potential for completely mineralizing organic pollutants into harmless byproducts under light irradiation [4-11]. However, the effectiveness of photocatalysis largely depends on the development of photocatalysts with enhanced light absorption [7], charge separation efficiency, and surface activity [8,9].

Carbon dots (CDs) have gained considerable attention as metalfree, eco-friendly, highly tunable nanomaterials with excellent optical properties and chemical stability [10,12]. Various biomass sources, including coffee grounds [13], orange peels [14], and sugarcane bagasse [15], have been explored as carbon precursors in line with the principles of green chemistry. However, most of these precursors are complex mixtures, making it challenging to control the carbon composition and doping efficiency precisely. In contrast, pure caffeine, a major alkaloid component of coffee, offers a structurally well-defined, nitrogen-rich organic molecule that can serve as a reproducible and controllable green precursor for synthesizing CDs. This opens new opportunities for tailoring the electronic properties of CDs for photocatalytic applications. Due to their unique electronic structure, CDs can act as efficient photocatalysts or photosensitizers, facilitating light-driven degradation of pollutants. However, pristine CDs often suffer from a wide bandgap energy and rapid charge recombination, which limits their photocatalytic efficiency [16,17]. To overcome these limitations, heteroatom doping has been widely explored as an effective strategy to enhance catalytic performance [7,11,16]. By introducing elements such as nitrogen, sulfur, phosphorus, and boron, heteroatom doping can significantly alter the electronic structure, improve charge carrier mobility, and increase the surface reactivity of CDs [18]. In particular, sulfur-doped carbon dots (S-doped CDs) have been demonstrated to be highly effective in modifying the band structure, enhancing charge separation, and promoting the generation of reactive oxygen species (ROS), which are crucial for photocatalytic activity [16,18]. The presence of sulfur atoms also facilitates the formation of additional defect sites and mid-gap states, improving light absorption and catalytic efficiency [7].

This study presents a novel and environmentally friendly synthetic approach for S-doped CDs using caffeine as a carbon precursor, sodium sulfide as the sulfur source, and ethylene glycol (EG) as the reaction

<sup>&</sup>lt;sup>1</sup> Department of Chemistry, Faculty of Science, Silpakorn University, Nakorn Pathom, 73000, Thailand

<sup>&</sup>lt;sup>2</sup> Pharmaceutical Development of Green Innovations Group (PDGIG), Department of Industrial Pharmacy, Faculty of Pharmacy, Silpakorn University, Nakhon Pathom, 73000, Thailand

<sup>&</sup>lt;sup>3</sup> Department of Physics, Faculty of Science, Silpakorn University, Nakhon Pathom, 73000, Thailand

<sup>\*</sup>Corresponding author e-mail: suwanchawalit c@su.ac.th

medium under solvothermal conditions. To the best of our knowledge, this specific combination of materials and conditions has not been previously reported. The structural, optical, and electronic properties of the synthesized CDs were systematically analyzed to evaluate the impact of sulfur doping on their photocatalytic performance. The photocatalytic performance of S-doped CDs was evaluated through the degradation of a model dye pollutant under UV irradiation, and the effects of sulfur doping on adsorption capacity, charge separation, and photocatalytic efficiency were examined. Furthermore, radical scavenger experiments were conducted to identify the dominant reactive species involved in the degradation process, proposing a photocatalytic mechanism. To the best of our knowledge, this work is one of the earliest studies to utilize pure caffeine as a molecular carbon and nitrogen source for synthesizing S-doped CDs via a solvothermal approach [19,20]. This strategy offers enhanced control over precursor composition and doping efficiency, distinguishing it from previous research that employed crude coffee waste materials. The findings from this work highlight the potential of S-doped CDs synthesized from caffeine as an efficient and sustainable photocatalyst for wastewater treatment and environmental remediation.

# 2. Experimental

## 2.1 Materials

All Chemicals used in this study were reagent grade, including caffeine anhydrous (C<sub>8</sub>H<sub>10</sub>N<sub>4</sub>O<sub>2</sub>, srlchem, 98%.), ethylene glycol (C<sub>2</sub>H<sub>6</sub>O<sub>2</sub>, Fisher chemical, 99.95%), sodium sulfide (Na<sub>2</sub>S,-Honeywell, 98%), ethylene diamine tetra acetic acid (EDTA, TPC, 99.5%), indigo carmine (Himedia), 1,4-Benzoquinone (Acrosr organics), *t*-butanol (Fluka chemicals) were used without purification.

# 2.2 Synthesis of S-doped CDs

A set of solutions was prepared by dissolving 1 g of caffeine along with varying amounts of Na<sub>2</sub>S (0.5 g, 1 g, and 2 g) in a 100 mL mixture of deionized (DI) water and EG in a 1:1 volume ratio to synthesize S-doped CDs. Undoped CDs were prepared under identical conditions, excluding Na<sub>2</sub>S, for comparison. To distinguish the samples, they were labeled as CDs (undoped), 0.5S-CDs (0.5 g Na<sub>2</sub>S), 1S-CDs (1 g Na<sub>2</sub>S), and 2S-CDs (2 g Na<sub>2</sub>S). These abbreviations will be used consistently throughout this paper. Each solution underwent sonication for 20 min before being transferred into autoclaves for a solvothermal reaction at 180°C for 24 h. The obtained CDs and S-doped CDs were purified by filtration using a 0.22  $\mu m$  filter and dialysis for 24 h, with periodic water replacement to remove unreacted precursors and impurities. Finally, the purified CDs dispersions were stored in a refrigerator for future use.



Figure 1. Photograph for the synthesis of S-doped CDs.

# 2.3 Characterizations

WONGWAEN, G., et al.

The size and shape of CDs were characterized using transmission electron microscopy (TEM) with a JEOL/JEM-3100F model. X-ray diffraction (XRD) analysis was employed to investigate the phase composition and crystalline structure of the samples, using a Malvern Panalytical Aeris diffractometer with Cu  $K_{\alpha}$  radiation ( $\lambda = 1.5406 \text{ Å}$ ), operated at 40 kV and 30 mA. The diffraction patterns were recorded over a 20 range of 5° to 80°, with a step size of 0.02° and a scan speed of approximately 1° min<sup>-1</sup>. The chemical bonds and functional groups were analyzed using X-ray photoelectron spectroscopy (XPS) with a Kratos Axis Ultra spectrometer and a monochromatic Al Kα source at 1486.7 eV. Fourier-transformed infrared (FT-IR) spectra were recorded on a PerkinElmer Spectrum Bx spectrophotometer in the range of 400 cm<sup>-1</sup> to 4000 cm<sup>-1</sup> using the attenuated total reflectance (ATR) technique. UV-Vis absorption spectra were obtained using a Shimadzu UV-2401 spectrophotometer. At the same time, fluorescence spectra were recorded using a fluorescence spectrophotometer (PerkinElmer LS55 luminescence spectrometer) with an excitation wavelength of 365 nm. For both measurements, 10 µL of the carbon dot solution was diluted in 6 mL of deionized water prior to analysis.

# 2.4 Photocatalytic activity

Indigo carmine (IC) was selected as the model dye for the experiment, prepared at a concentration of  $2.5 \times 10^{-5}$  M in a total volume of 50 mL. 2.5 mL of CDs were added to this dye solution to act as the photocatalyst. The mixture was left in the dark for 60 min to achieve adsorption equilibrium between the dye and the CDs.

After the dark incubation period, the solution was exposed to UV light or visible light for 4 h. During UV and visible exposure (blacklight, 20 W [21]; Daylight, 9 W), aliquots were collected at 30 min intervals, and the absorbance of the IC dye solution was measured at 610 nm using a UV-vis spectrophotometer.

$$\%Degradation = \frac{A_0 - A_t}{A_0} \times 100 \tag{1}$$

where  $A_0$  represents the initial absorbance at 610 nm before UV exposure, and  $A_t$  is the absorbance at 610 nm at a specific time t during the UV or visible exposure.

This process enables the evaluation of the photocatalytic efficiency of CDs in degrading IC under UV light and visible light conditions.

# 2.5 Radical test

Selective scavengers are employed to capture specific free radicals, allowing the identification of those involved in the reaction. A decrease in photocatalytic efficiency indicates the contribution of each radical to the process. For instance, *t*-butanol serves as a scavenger for hydroxyl radicals ('OH), p-benzoquinone is used to capture superoxide radicals ('O<sub>2</sub>–), and EDTA acts as a trap for photogenerated holes (h<sup>+</sup>). To experiment, 5 mL of the selected scavenger is added to a 50 mL IC solution with a concentration of  $2.5 \times 10^{-5}$  M. Subsequently, 2.5 mL of CDs is introduced, and the mixture is kept in the dark for 60 min to allow adsorption equilibrium. The reaction is then initiated by exposing

the mixture to UV light for 4 h, with samples collected every  $30 \, \text{min}$  to track the degradation process. The absorbance of each sample is measured at  $610 \, \text{nm}$  to assess the effect of each scavenger on photocatalytic activity.

## 3. Results and discussion

# 3.1 Optical and structural properties of S-doped CDs

Figure 2 shows the visual appearance of S-doped CDs under daylight (a) and UV light at 365 nm (b), revealing the impact of sulfur incorporation on their optical properties. Under daylight, all CDs solutions exhibit a light yellow to pale brown color, indicating the formation of graphitic or amorphous carbon structures with good dispersion in the solvent. Under UV light, all samples display bright blue fluorescence, with 0.5S-CDs and 1S-CDs exhibiting higher intensity than CDs and 2S-CDs, indicating that sulfur doping enhances radiative recombination through the formation of new emissive states or passivating defects.

The PL spectra of CDs and S-doped CDs at an excitation wavelength of 365 nm, as shown in Figure 3, demonstrate a significant enhancement in fluorescence intensity compared to undoped CDs, with 0.5S-CDs exhibiting the highest emission, followed by 1S-CDs, 2S-CDs, and CDs. This increase in intensity (420 nm to 450 nm range) is attributed to surface passivation, reduced non-radiative recombination, and the introduction of sulfur functional groups (C–S, C=O, SO<sub>x</sub>), which create additional electronic states that enhance radiative transitions [22-24]. However, a slight fluorescence quenching is observed at higher sulfur content (2S-CDs) due to the excessive presence of defect states acting as non-radiative recombination centers [25,26].

The UV-Vis absorption spectra of caffeine-derived CDs, as shown in Figure 4, highlight the structural transformation of caffeine after solvothermal synthesis. Caffeine, a nitrogen-rich organic molecule, contains multiple C=C, C=N, and C=O bonds, crucial in forming CDs. The observed absorption features in the pristine caffeine spectrum differ from those of the synthesized CDs, indicating significant changes in molecular structure due to high-temperature treatment and carbonization. The spectra show a strong absorption peak in the 200 nm to 250 nm region, corresponding to the  $\pi \to \pi^*$  transition of C=C bonds in the aromatic and conjugated domains of the CDs [9,27]. This peak is observed in all samples, indicating that the fundamental graphitic structure remains preserved despite sulfur doping. Another peak appears around 270 nm to 300 nm, attributed to the  $\pi \to \pi^*$ transition of C=N bonds. This absorption suggests the presence of nitrogen-containing groups, which may originate from the caffeine precursor [9,16,18,21-30]. A weaker absorption feature is detected near 350 nm to 400 nm, corresponding to the n  $\rightarrow \pi^*$  transition of C=O bonds from oxygen-containing functional groups on the CD surface [31]. This transition is typically associated with surface functionalization and defect states, which can influence the optical properties of CDs. Notably, a new absorption feature appears around 320 nm to 350 nm, attributed to the  $n \to \pi^*$  transition of C-S bonds. This transition confirms that sulfur atoms are successfully incorporated into the structure of CDs, likely replacing oxygen atoms in carbonyl groups to form thiocarbonyl (-C-S) functional groups [32]. The C-S transition is a distinguishing feature of sulfur doping and contributes to changes in the electronic properties of the CDs. This electronic transition not only confirms the structural incorporation of sulfur but also indicates modifications in the electronic distribution, which may influence the optical absorption behavior and photocatalytic activity of the S-doped CDs.

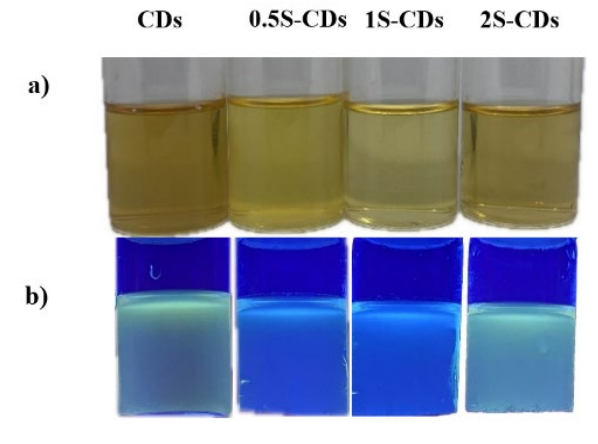


**Figure 2.** Photograph of CDs solution in daylight (a), and UV light (365 nm) (b) with various amounts of sulfur doping.

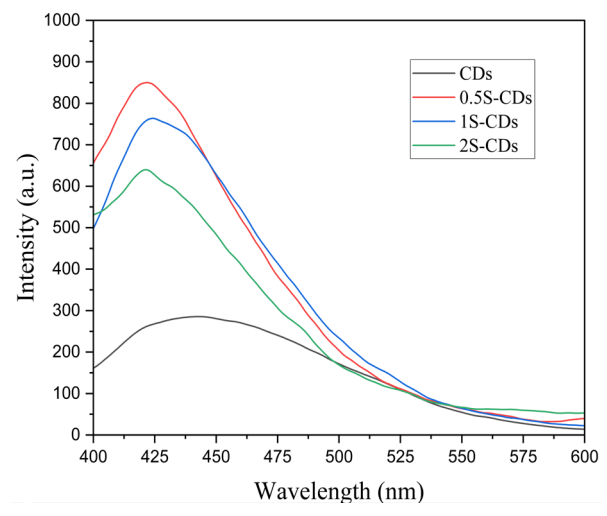


**Figure 3.** Photoluminescence of CDs with differences in sulfur content at excitation 365 nm.

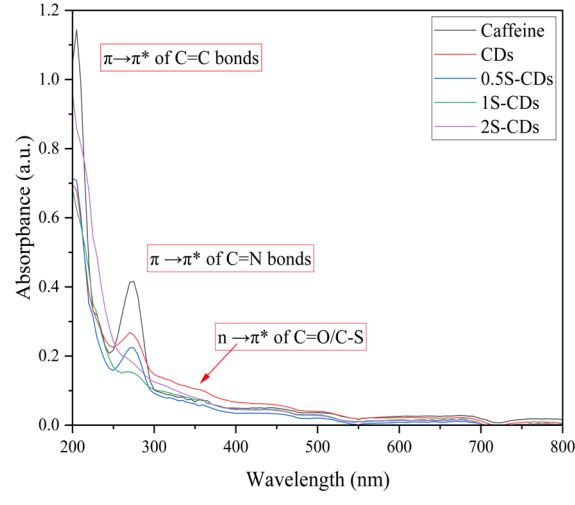


Figure 4. UV-Vis spectra of CDs with Caffeine and CDs with different sulfur content.

The XRD patterns of the undoped CDs and S-doped CDs (0.5S-CDs, 1S-CDs, and 2S-CDs) are presented in Figure 5. All samples exhibit broad diffraction peaks centered at approximately  $2\theta = 22^{\circ}$ to 26°, which are indicative of the (002) plane of disordered graphitic carbon. This characteristic peak reflects the presence of an amorphous or turbostratic structure commonly observed in carbon-based nanomaterials, including CDs [33,34]. Upon doping with sulfur, a gradual increase in the intensity of the diffraction peaks is observed, particularly in the 2S-CDs sample, which shows the most pronounced peak. This enhancement suggests an increase in the degree of structural ordering and possible partial graphitization. The presence of sulfur heteroatoms may promote the rearrangement of carbon layers by modifying the electronic environment and introducing localized structural defects, leading to improved crystallinity [35]. Furthermore, the peak broadening observed across all samples implies that the synthesized CDs retain a predominantly amorphous structure with limited graphitic domains. The subtle variations in peak position and intensity with increasing sulfur content can be attributed to lattice distortion and strain effects resulting from sulfur incorporation into the carbon matrix. These results confirm the successful doping of sulfur and its influence on the structural characteristics of CDs.

The TEM images in Figure 6 reveal that CDs and 2S-CDs exhibit quasi-spherical morphology with well-dispersed nanoparticles, indicating successful synthesis. The presence of lattice fringes in both samples, with an interlayer spacing of approximately 0.20 nm to 0.21 nm, corresponds to the (100) and (101) plane of carbon, confirming the partially graphitic nature of the CDs [36-39]. 2S-CDs exhibits increased structural disorder compared to CDs, as evidenced by less defined lattice fringes, suggesting that sulfur incorporation introduces defects and heteroatom-induced distortions within the carbon framework [38-41]. Despite these modifications, the retention of graphitic domains in 2S-CDs suggests that sulfur doping occurs mainly at surface functional sites rather than disrupting the core sp<sup>2</sup> carbon network [39-42]. In addition, the particle size distribution of CDs was illustrated for CDs in Figure 6(c) and for 2S-CDs in Figure 6(d). It was found that the average particle size of CDs was approximately 4.93 nm, while that of 2S-CDs was approximately 5.14 nm.

The Tauc plot in Figure 7 illustrates the optical band gap of CDs and S-doped CDs as determined from UV-Vis spectroscopy, with band gap values estimated using Tauc's equation

$$(\alpha h v)^n = A(h v - E_g) \tag{2}$$

where  $\alpha$  is the absorption coefficient, hv is the photon energy, A is a constant, and  $E_g$  is the optical band gap. The nature of the electronic transition determines the exponent n. For CDs that exhibit direct transitions due to their quantum confinement and graphitic-like domains, n=2 is commonly used [24,27,36,43]. The results indicate that pure CDs exhibit the highest band gap, while increasing sulfur doping progressively reduces the band gap, with 2S-CDs showing the lowest band gap energy, suggesting the introduction of mid-gap states that facilitate electronic transitions at lower energies [39,42]. This band gap narrowing is attributed to heteroatom-induced defect states and enhanced electronic delocalization, which modifies the electronic structure of the CDs [43,44].

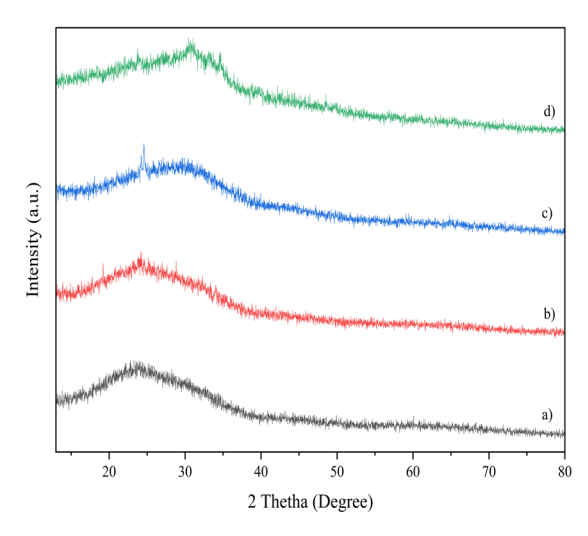


Figure 5. XRD Patterns of CDs Samples (a) CDs, (b) 0.5S-CDs, (c) 1S-CDs, and (d) 2S-CDs.

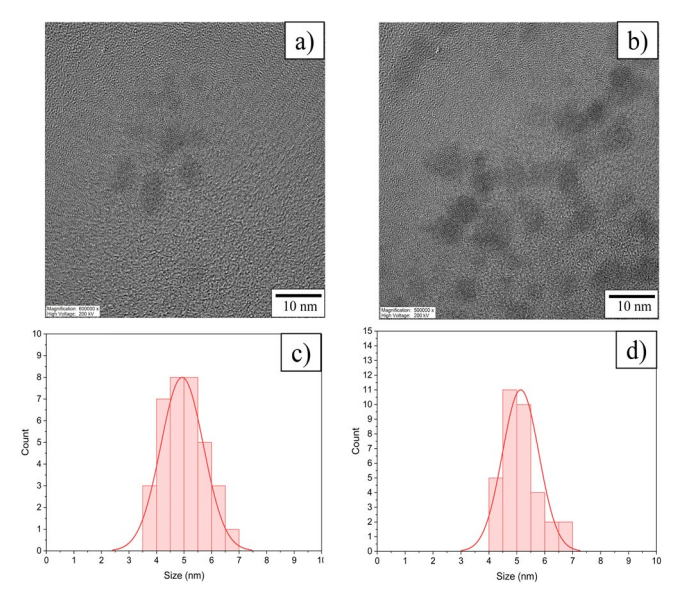


Figure 6. TEM image of CDs samples (a) CDs, (b) 2S-CDs and size distribution of (c) CDs, and (d) 2S-CDs.

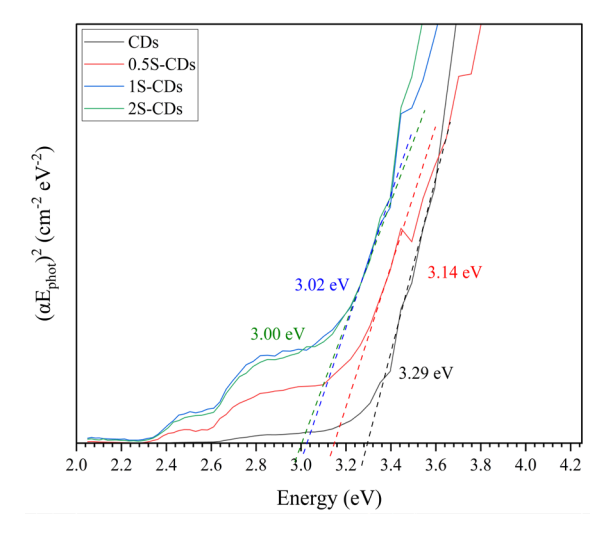


Figure 7. Tauc plot for the optical band gap of CDs and S-doped CDs.

Table 1. Bandgap energy of synthesized CDs with different amounts of sulfur doping.

Samples	Bandgap Energy (eV)
CDs	3.29
0.5S-CDs	3.14
1S-CDs	3.02
2S-CDs	3.00

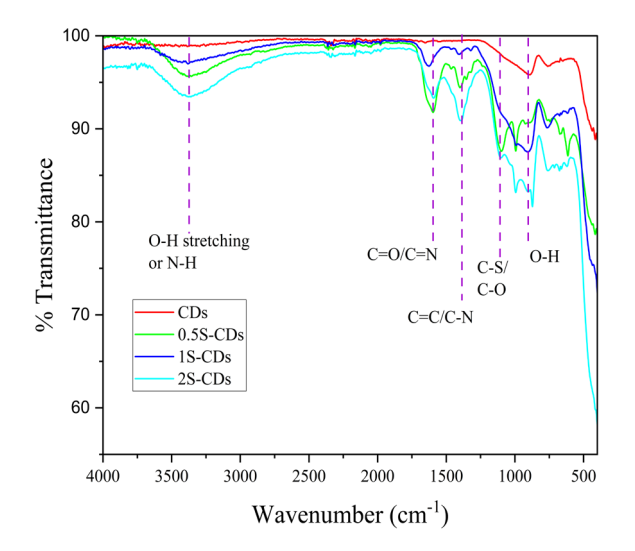


Figure 8. FT-IR spectra of CDs with different amounts of sulfur doping.

Table 1 presents the calculated band gap energy of S-doped CDs, showing a progressive decrease in  $E_g$  with increasing sulfur content, indicating the impact of sulfur incorporation on the electronic structure of CDs. Pure CDs and 0.5S-CDs exhibit the highest band gap, 3.29 eV and 3.14 eV, respectively, suggesting that at low sulfur doping levels, the electronic structure remains relatively unchanged [45,46]. However, a significant reduction in the band gap is observed in 1S-CDs (3.02 eV) and 2S-CDs (3.00 eV), confirming that sulfur doping introduces midgap states and enhances electronic delocalization, thereby facilitating electronic transitions at lower energy levels [39,44]. This trend aligns with previous studies, where sulfur doping modifies the density of states in heteroatom-doped CDs, leading to enhanced light absorption and improved charge carrier dynamics [42,47,48]. The results suggest that higher sulfur concentrations (1S-CDs and 2S-CDs) are required to induce significant electronic modifications, making sulfur doping an effective strategy for tuning the optical properties of CDs.

## 3.2 Surface analysis

The FT-IR spectra in Figure 8 confirms the presence of key functional groups in S-doped CDs, highlighting the impact of sulfur incorporation on their surface chemistry. A broad peak at 3300 cm<sup>-1</sup> to 3500 cm<sup>-1</sup> corresponds to O–H and N–H stretching, indicating the presence of hydroxyl and amine groups that enhance the hydrophilicity of CDs [26,49]. The peaks at ~1650 cm<sup>-1</sup> and ~1580 cm<sup>-1</sup> are assigned to C=O and C=C stretching, confirming the presence of carbonyl groups and the partial graphitic nature of the CDs [50]. Sulfur incorporation is evident from the appearance of C–S stretching (~1080 cm<sup>-1</sup> to 1200 cm<sup>-1</sup>), confirming successful sulfur doping [26,28], while the peak at ~1380 cm<sup>-1</sup> suggests the retention of C–N bonds from the precursor material [26,28,51]. Notably, the peaks around 1000 cm<sup>-1</sup> to 1050 cm<sup>-1</sup>

correspond to oxidized sulfur species  $(SO_x)$  functional groups, such as sulfone  $(-SO_2)$  or sulfate  $(-SO_4)$ , indicating partial oxidation of sulfur during synthesis. The observed changes in C=O, C=S, and  $SO_x$  functional groups with increasing sulfur content suggest that sulfur incorporation significantly modifies the chemical environment and electronic properties of CDs.

XPS was employed to elucidate the elemental composition and chemical-bonding states of both the precursor (caffeine) and the synthesized S-doped CDs (2S-CDs), as illustrated in Figure 9. The survey spectra show C 1s, O 1s, and N 1s signals in both samples, whereas an additional S 2p peak appears exclusively in the 2S-CDs spectrum, confirming the successful incorporation of sulfur during solvothermal synthesis [26,52]

In the high-resolution C 1s spectrum of caffeine, four components are observed at 284.5 eV (C–C/C=C) [16,53], 285.7 eV (C–N) [16,53-55], 286.7 eV (O=C–N) [53-55] and 288.5 eV (C=O) [55,56], consistent with its molecular structure. After carbonization, the C 1s spectrum of 2S-CDs retains these features. It displays an additional peak at 284.9 eV, which can be assigned to C–S bonding, indicating the covalent integration of sulfur into the carbon lattice.

The N 1s spectrum of caffeine is dominated by pyrrolic nitrogen (~399.9 eV) [55], graphitic-like nitrogen (~401.0 eV) [26] and C-N-C (~398.7 eV) [16]. By contrast, the 2S-CDs exhibit three nitrogen species pyridinic N at 398.7 eV [55], pyrrolic N at 399.7 eV [55] and graphitic N at 401.0 eV [41] implying a rearrangement of nitrogen functionalities during solvothermal treatment that is known to enhance electronic conductivity and charge-separation efficiency in photocatalytic systems [16,26,30].

The O 1s spectra further substantiate surface modification: caffeine presents peaks at 531.0 eV (C–O/C = O) [55], 532.7 eV (C–OH/C–O–C) [55] and 534.2 eV (O–H) [55,57,58], suggesting the presence of oxygencontaining functional groups contributing to solubility and reactivity. Notably, whereas the 2S-CDs display an additional peak at 532.9 eV attributable to S–O bonding environments such as sulfone or sulfate groups, providing compelling evidence for the formation of oxidized sulfur species during synthesis [59], such as sulfone (–SO<sub>2</sub>–) or sulfate (–SO<sub>4</sub><sup>2–</sup>) functional groups. This observation confirms the presence of oxidized sulfur species on the carbon dot surface, further supporting the successful sulfur doping and partial surface oxidation that occurred during the synthesis process.

The S 2p spectrum of 2S-CDs exhibits two spin–orbit doublets. The first, centered at 164.1 eV  $(2p_{3/2})$  and 165.3 eV  $(2p_{1/2})$ , [16,26] corresponds to thiophene-like C–S–C bonds; the second, at 168.0 eV  $(2p_{3/2})$  and 169.3 eV  $(2p_{1/2})$  [16,26], is assigned to oxidized sulfur species  $(C-SO_x)$ , indicating partial oxidation of the dopant under solvothermal conditions [16,30,49,55,60,61]. Collectively, these XPS results confirm that caffeine, a nitrogen-rich molecular precursor, was successfully transformed into heteroatom-doped CDs through sulfur incorporation and the formation of new chemical bonds. The

coexistence of C–S and S–O functionalities, together with a reconfigured nitrogen environment, introduces active sites and defect states that are expected to enhance the optical and photocatalytic performance of the resulting 2S-CDs.

The XPS findings are consistent with the FT-IR, UV-Vis, and PL analyses, indicating the presence of C-S, C=O, and oxygenated

functional groups. Detecting C–S and SO<sub>x</sub> peaks in XPS aligns with FT-IR results. Additionally, the decrease in optical band gap observed in UV-Vis/Tauc plot analysis correlates with the chemical modifications detected by XPS, as sulfur incorporation introduces defect states and mid-gap energy levels, facilitating electronic transitions at lower energies [26,28].

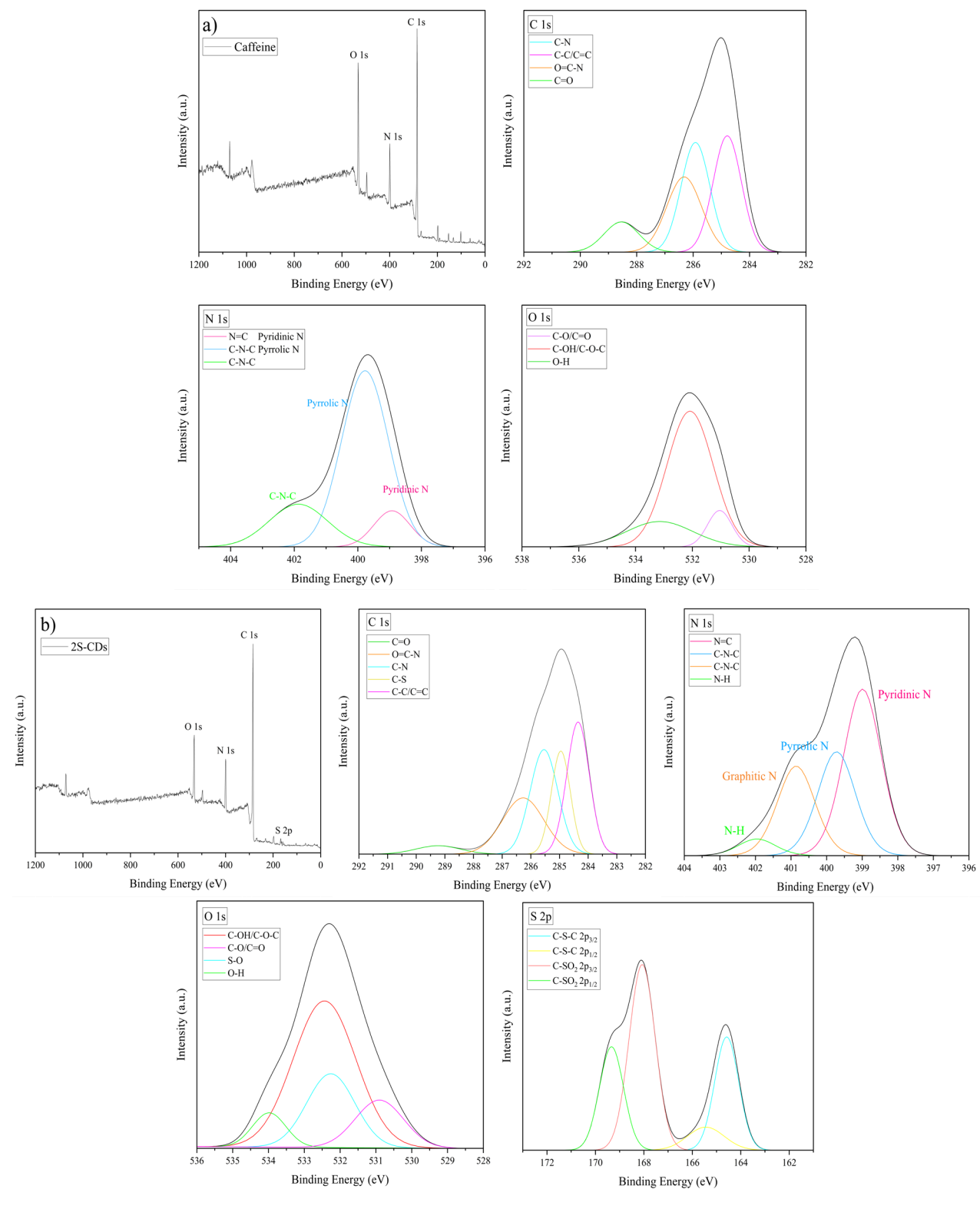


Figure 9. XPS spectra of a) Caffeine, and b) 2S-CDs.

# 3.3 Photocatalyst efficiency

The photocatalytic degradation of IC dye using S-doped CDs was systematically investigated, revealing that 2S-CDs exhibited the highest photocatalytic efficiency in UV light, achieving approximately 90% degradation within 240 min, as illustrated in Figure 10(a). This enhanced photocatalytic activity is primarily attributed to sulfur-induced defect states, which facilitate improved charge carrier separation [62], broaden the light absorption spectrum, and significantly reduce electronhole recombination processes [13,25]. Additionally, dark adsorption played a crucial role in the removal of IC dyes, as evidenced in Figure 11. Among the tested samples, 2S-CDs demonstrated the highest adsorption capacity (~75%), followed by 1S-CDs (~30%) and 0.5S-CDs (~10%). This trend is likely due to increased electrostatic interactions, the presence of functional surface groups such as –SO<sub>x</sub> and –COOH, and strong  $\pi$ - $\pi$  stacking interactions between the sp<sup>2</sup>-carbon domains of the CDs and the conjugated  $\pi$ -system of the IC dye molecules [50,63]. The high adsorption affinity of S-doped CDs toward indigo carmine dye effectively facilitates subsequent photocatalytic degradation, thereby significantly enhancing the overall photocatalytic efficiency.

Furthermore, the results presented in Figure 10(b), which evaluate photocatalytic degradation under visible light irradiation alone (i.e., in the absence of UV activation), emphasize the critical role of sulfur doping in enhancing visible-light-driven photocatalysis. Notably, 2S-CDs, containing the highest sulfur content, exhibited superior activity with approximately 40% IC degradation within the first 60 min. In contrast, 1S-CDs and 0.5S-CDs showed only moderate performance (~10% to 15%), while pristine CDs and the IC control sample displayed negligible degradation (less than 5%). These findings highlight the efficacy of sulfur doping in extending the optical absorption of CDs into the visible region and promoting more effective charge separation via defect and mid-gap states.

The exceptional performance of 2S-CDs under visible light is attributed to sulfur atoms introducing localized trap states, which reduce the bandgap and enhance absorption in the 400 nm to 700 nm range, thereby improving electron—hole pair generation under low-energy illumination. These results are aligned with prior studies reporting that sulfur doping significantly enhances photocatalytic activity by mitigating charge recombination and augmenting visible light harvesting capabilities [20, 64].

The rate constant (k) for IC degradation was calculated and is displayed in Figure 12. The degradation kinetics follow a pseudo-first-order model, which is described by the Langmuir-Hinshelwood kinetic Equation.

$$\ln\left(\frac{C_0}{Ct}\right) = kt$$
(3)

where  $C_0$  is the initial concentration of the dye,  $C_t$  is the concentration at time t, k is the rate constant (min<sup>-1</sup>), and t is the reaction time (min).

Here,  $C_0$  refers to the concentration of IC after reaching adsorption—desorption equilibrium in the dark, prior to light irradiation. Therefore, the decrease in  $C_1$  reflects the photocatalytic degradation only.

Among the samples, 2S-CDs exhibited the highest rate constant ( $\sim$ 0.0124 min<sup>-1</sup>), significantly outperforming undoped CDs. The increased reaction rate with sulfur doping is attributed to improved charge separation and enhanced generation of ROS, which accelerate dye decomposition by reducing electron-hole recombination and facilitating oxidation-reduction reactions [64].

To better understand the degradation pathway, radical trapping experiments were conducted (Figure 13), revealing that  ${}^{\bullet}O_2^-$ ,  ${}^{\bullet}OH$ , and photogenerated  $h^+$  play essential roles in the photocatalytic process. The degradation efficiency significantly decreased in the presence of benzoquinone ( ${}^{\bullet}O_2^-$  scavenger), t-butanol ( ${}^{\bullet}OH$  scavenger), and EDTA ( $h^+$  scavenger), indicating that all these reactive species are actively involved in IC dye degradation [65]. The oxidative species generated during the process can be ranked in order of significance as follows:  ${}^{\bullet}O_2^- > h^+ > {}^{\bullet}OH$ . These radicals are crucial for the degradation of IC dye through the photocatalytic process facilitated by the CDs.

$$E_{\rm CB} = X - E_{\rm e} - \frac{E_{\rm g}}{2}$$
 (4)

$$E_{\rm VB} = E_{\rm CB} + E_{\rm g} \tag{5}$$

In this study, the band edge positions of S-doped CDs (2S-CDs) were calculated using Mulliken electronegativity theory, which is commonly employed to estimate the valence band (VB) and conduction band (CB) edge potentials using the following Equations [66].

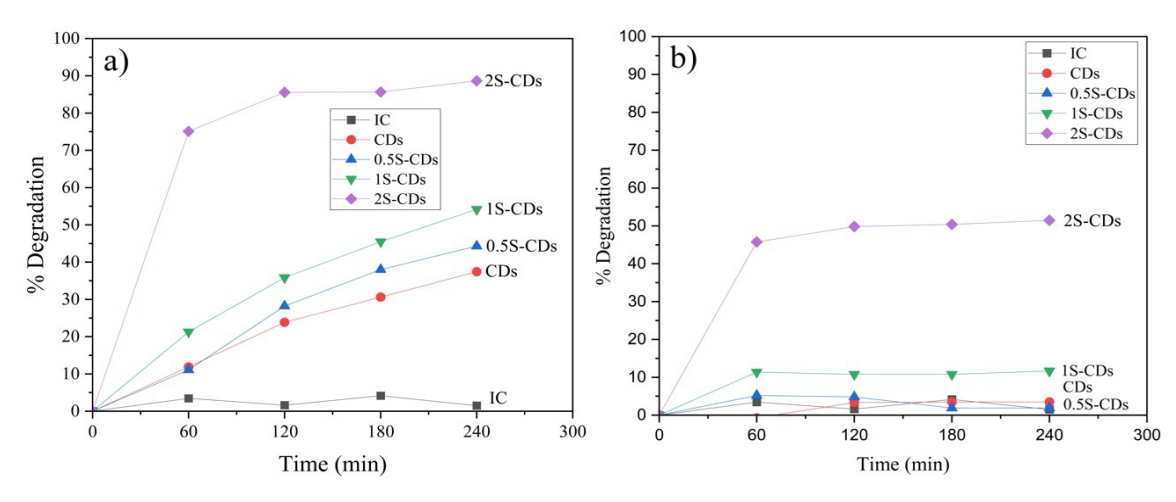


Figure 10. Photocatalytic efficiency of CDs with different amounts of sulfur doping under (a) UV light, and (b) Visible light.

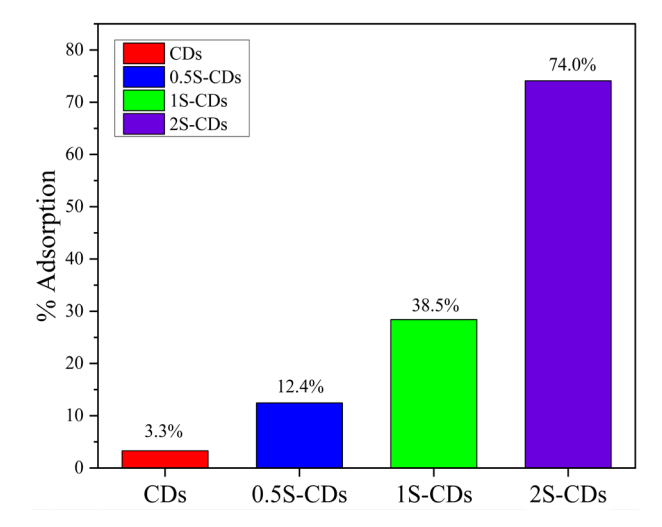


Figure 11. Adsorption efficiency of CDs with different amounts of sulfur doping in the dark.

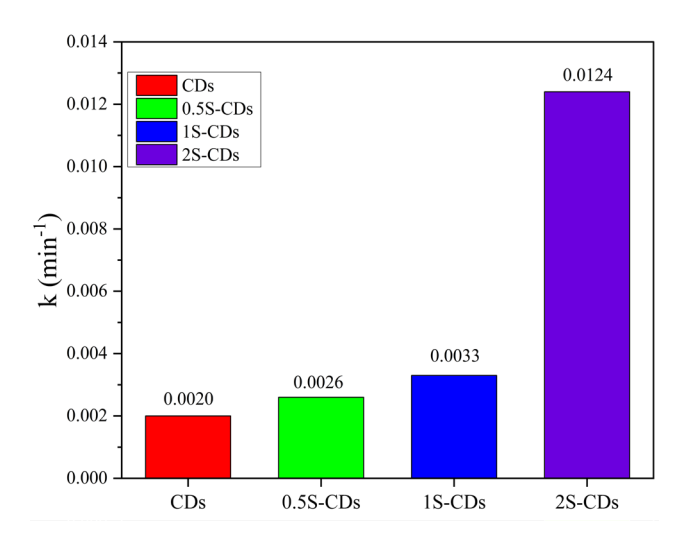
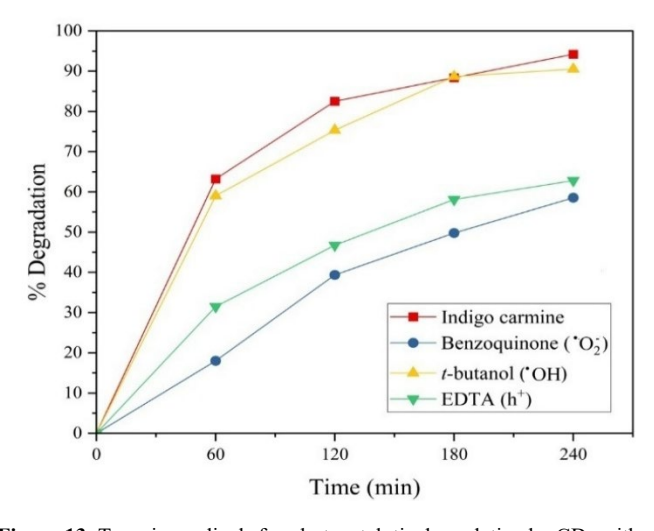


Figure 12. Kinetic rate constants for photocatalytic degradation by CDs with different amounts of sulfur doping.



**Figure 13.** Trapping radicals for photocatalytic degradation by CDs with different amounts of sulfur doping under UV light.

where X is the Mulliken electronegativity of the material, calculated as the weighted average of the electronegativity values of the constituent elements (C, N, O, and S), which in this case is approximately 5.35 eV, derived from XPS data [67]. E<sub>e</sub> represents the energy of free electrons on the vacuum scale, typically valued at 4.5 eV. E<sub>g</sub> is the optical band gap energy obtained from UV–Vis spectroscopy, with a value of 3.00 eV for 2S-CDs.

Based on the calculation, the conduction band (CB) and valence band (VB) edge positions of 2S-CDs are -0.65 eV and  $\pm 2.35$  eV, respectively, on the vacuum scale. When referenced against the redox potential of relevant reactive species, these values suggest a favorable electronic structure for radical generation. Specifically, the CB position at -0.65 eV is more negative than the reduction potential of molecular oxygen to superoxide radical (O2/'O2'  $\approx -0.33$  eV vs. NHE), indicating that photogenerated electrons possess sufficient energy to reduce O2 to 'O2" [66]. Likewise, the VB position at  $\pm 2.35$  eV is higher than the oxidation potential required for hydroxyl radical generation from H2O or OH" ( $\pm 1.99$  eV), suggesting that photogenerated holes are sufficiently oxidative to produce 'OH [68].

The calculated band edge potentials of 2S-CDs are well-aligned with the proposed mechanism for IC degradation via advanced oxidation processes (AOPs). The generation of highly reactive 'OH and 'O<sub>2</sub>-radicals facilitates the oxidative cleavage of dye molecules, resulting in efficient degradation [69].

Based on these findings, a proposed photocatalytic mechanism is shown in Figure 14. Under UV excitation, electrons are excited from the VB to the CB, generating electron-hole pairs. The photoinduced electrons in the CB react with  $O_2$  to generate  ${}^{\bullet}O_2{}^{-}$ , while holes ( $h^{+}$ ) in the VB oxidize  $H_2O$  to form  ${}^{\bullet}OH$ , both of which attack IC dye molecules, leading to complete mineralization into  $CO_2$  and  $H_2O$  [13,28,70]. The reactions involved in the photocatalytic process are summarized as follows.

S-doped CDs + 
$$h\nu \rightarrow e^- + h^+$$
 (6)

$$O_2 + e^- \rightarrow {}^{\bullet}O_2^- \tag{7}$$

$$H_2O + h^+ \rightarrow {}^{\bullet}OH + H^+$$
 (8)

IC dye + 
$${}^{\bullet}OH + {}^{\bullet}O_2^- \rightarrow Degradation products$$
 (9)

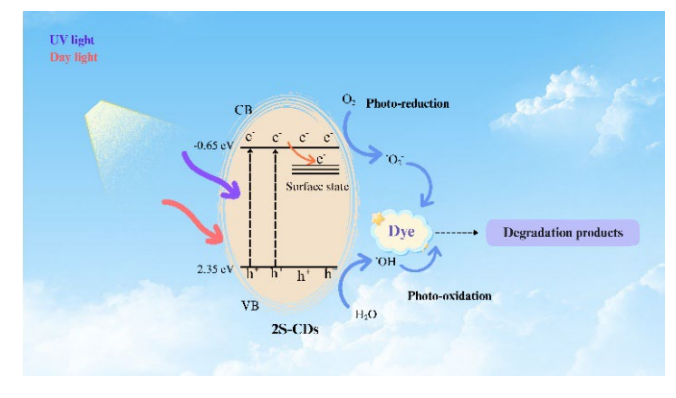


Figure 14. Proposed photocatalytic mechanism of S-doped CDs.

# 4. Conclusion

This study successfully synthesized S-doped CDs via a solvothermal method using caffeine as a carbon precursor and Na2S as a sulfur source. Characterizations using XRD, TEM, XPS, FT-IR, UV-Vis, and PL spectroscopy confirmed the successful incorporation of sulfur, resulting in modified electronic structures, enhanced surface functionalization, and a reduced bandgap energy from 3.29 eV (undoped CDs) to 3.00 eV (2S-CDs). The photocatalytic performance of S-doped CDs was evaluated for IC dye degradation, with 2S-CDs exhibiting the highest degradation efficiency (~90% within 240 min under UV irradiation; ~50% within 240 min under visible irradiation) due to improved charge carrier separation, defect-state-mediated electron transfer, and ROS generation. Adsorption studies revealed that 2S-CDs exhibited the highest dye adsorption (~75%), attributed to electrostatic interactions, surface functionalization ( $-SO_x$ , -COOH), and  $\pi-\pi$  stacking with IC dye molecules, which facilitated efficient photocatalysis. This dual function leads to a synergistic adsorption-photocatalysis mechanism, offering promising potential for efficient and sustainable dye degradation in aqueous environments. Radical scavenger experiments confirmed that 'O<sub>2</sub>-, 'OH, and photogenerated h<sup>+</sup> played critical roles in dye degradation. Band-edge calculations verified that the energetic positions of the conduction and valence bands favor the formation of 'OH and \*O<sub>2</sub>-radicals upon irradiation. These findings demonstrate that S-doped CDs synthesized from caffeine offer a sustainable and efficient photocatalyst for wastewater treatment. Future work will focus on evaluating the performance of S-doped CDs in more complex systems, including simulated or real wastewater containing competing ions and mixed organic pollutants, to assess their practical applicability in environmental remediation. In addition, to enhance reusability, future development will explore the immobilization of S-doped CDs onto solid supports (e.g., TiO<sub>2</sub>, ZnO, BiOI), enabling easier recovery and recyclability in practical applications.

# Acknowledgments

The author would like to thank the Faculty of Science, Silpakorn University, Nakhon Pathom, Thailand, for financial support (Grant No. SRIF-JRG-2568-05).

## Reference

- [1] M. Berradi, R. Hsissou, M. Khudhair, M. Assouag, O. Cherkaoui, A. El Bachiri, and A. El Harfi, "Textile finishing dyes and their impact on aquatic environs," *Heliyon*, vol. 5, p. e02711, 2019.
- [2] M. Tripathi, S. Singh, S. Pathak, J. Kasaudhan, A. Mishra, S. Bala, D. Garg, R. Singh, P. Singh, P. K. Singh, A. K. Shukla, and N. Pathak, "Recent strategies for the remediation of textile dyes from wastewater: A systematic review, *Toxics*, vol. 11 p. 940, 2023.
- [3] O. F. Kayode, C. Luethi, and E. R. Rene, "Management recommendations for improving decentralized wastewater treatment by the food and beverage industries in nigeria," *Environments*, vol. 5, p. 41, 2018.

- [4] Z. Eren, "Degradation of an azo dye with homogeneous and heterogeneous catalysts by sonophotolysis, *CLEAN Soil Air Water*, vol. 40, pp. 1284-1289, 2012.
- [5] Y. Yao, H. Zhang, K. Hu, G. Nie, Y. Yang, Y. Wang, X. Duan, and S. Wang, "Carbon dots based photocatalysis for environmental applications," *Journal of Environmental Chemical Engineering*, vol. 10, p. 107336, 2022.
- [6] M. Sha, H. Anwar, F. Musthafa, H. Al-Lohedan, S. Alfarwati, J. Rajabathar, J. Alahmad, J.-J. Cabibihan, M. Karnan, and K. k. Sadasivuni, "Photocatalytic degradation of organic dyes using reduced graphene oxide (rGO)," *Scientific Reports*, vol. 14, p. 3608, 2024.
- [7] Z. Peng, Y. Zhou, C. Ji, J. Pardo, K. J. Mintz, R. R. Pandey, C. C. Chusuei, R. M. Graham, G. Yan, and R. M. Leblanc, "Facile synthesis of "boron-doped" carbon dots and their application in visible-light-driven photocatalytic degradation of organic dyes," *Nanomaterials*, vol. 10, p. 1560, 2020.
- [8] N. Ramesh, C. W. Lai, M. R. B. Johan, S. M. Mousavi, I. A. Badruddin, A. Kumar, G. Sharma, and F. Gapsari, "Progress in photocatalytic degradation of industrial organic dye by utilising the silver doped titanium dioxide nanocomposite," *Heliyon*, vol. 10, p. e40998, 2024.
- [9] Y. Gong, B. Yu, W. Yang, and X. Zhang, Phosphorus, and nitrogen co-doped carbon dots as a fluorescent probe for realtime measurement of reactive oxygen and nitrogen species inside macrophages," *Biosensors and Bioelectronics*, vol. 79 pp. 822-828, 2016.
- [10] Y. Wang, and A. Hu, "Carbon quantum dots: synthesis, properties and applications," *Journal of Materials Chemistry C*, vol. 2, pp. 6921-6939, 2014.
- [11] Y. Pan, S. Sanati, R. Abazari, A. Jankowska, J. Goscianska, V. Srivastava, U. Lassi, J. Gao, "Vanadium- and manganesebased metal-organic frameworks for potential environmental and catalysis applications," *Coordination Chemistry Reviews*, vol. 522, p. 216231, 2025.
- [12] V. L. John, Y. Nair, and T. P. Vinod, "Doping and surface modification of carbon quantum dots for enhanced functionalities and related applications," *Particle & Particle Systems Characterization*, vol. 38, p. 2100170, 2021.
- [13] Y. Zhu, X. Deng, J. Chen, Z. Hu, and F. Wu, "Coffee grounds-derived carbon quantum dots as peroxidase mimetics for colorimetric and fluorometric detection of ascorbic acid," *Food Chemistry*, vol. 429, p. 136957, 2023.
- [14] C. Michenzi, A. Proietti, M. Rossi, C. Espro, V. Bressi, F. Vetica, B. Simonis, and I. Chiarotto, "Carbon nanodots from orange peel waste as fluorescent probes for detecting nitrobenzene," *RSC Sustainability*, vol. 2, pp. 933-942, 2024.
- [15] T. Selvarathinam, and R. S. Dhesingh, "Green synthesis of highly fluorescent carbon quantum dots from sugarcane bagasse pulp," *Applied Surface Science*, vol. 390, pp. 435-443, 2016.
- [16] A. Saengsrichan, C. Saikate, P. Silasana, P. Khemthong, W. Wanmolee, J. Phanthasri, S. Youngjan, P. Posoknistakul, S. Ratchahat, N. Laosiripojana, K. C. W. Wu, and C. Sakdaronnarong, "The role of N and S doping on photoluminescent characteristics of carbon dots from palm bunches for fluorimetric sensing of

- Fe<sup>3+</sup> Ion," *International Journal of Molecular Sciences*, vol. 23, p. 5001, 2022.
- [17] Y. Zhou, A. E. ElMetwally, J. Chen, W. Shi, E. K. Cilingir, B. Walters, K. J. Mintz, C. Martin, B. C. L. B. Ferreira, W. Zhang, S. D. Hettiarachchi, L. F. Serafim, P. L. Blackwelder, A. H. Wikramanayake, Z. Peng, R. M. Leblanc, Gel-like carbon dots: A high-performance future photocatalyst," *Journal of Colloid and Interface Science*, vol. 599, pp. 519-532, 2021.
- [18] M. Azami, and J. Wei, M. Valizadehderakhshan, A. Jayapalan, O. O. Ayodele, K. Nowlin, "Effect of doping heteroatoms on the optical behaviors and radical scavenging properties of carbon nanodots," *The Journal of Physical Chemistry C*, vol. 127, pp. 7360-7370, 2023.
- [19] S. Mohandoss, S. Ganesan, S. Palanisamy, S. You, K. Velsankar, S. Sudhahar, H.-M. Lo, and Y. R. Lee, "Nitrogen, sulfur, and phosphorus co-doped carbon dots-based ratiometric chemosensor for highly selective sequential detection of Al<sup>3+</sup> and Fe<sup>3+</sup> ions in logic gate, cell imaging, and real sample analysis," *Chemosphere*, vol. 313, p. 137444, 2023.
- [20] S. Zhu, Q. Meng, L. Wang, J. Zhang, Y. Song, H. Jin, K. Zhang, H. Sun, H. Wang, and B. Yang, "Highly Photoluminescent carbon dots for multicolor patterning, sensors, and bioimaging," *Angewandte Chemie International Edition*, vol. 52, pp. 3953-3957, 2013.
- [21] C. Suwanchawalit, and S. Wongnawa, Influence of calcination on the microstructures and photocatalytic activity of potassium oxalate-doped TiO<sub>2</sub> powders," *Applied Catalysis A: General*, vol. 338, pp. 87-99, 2008.
- [22] L. Ai, Y. Yang, B. Wang, J. Chang, Z. Tang, B. Yang, and S. Lu, Insights into photoluminescence mechanisms of carbon dots: advances and perspectives," *Science Bulletin*, vol. 66, pp. 839-856, 2021.
- [23] H. Yi, J. Liu, J. Yao, R. Wang, W. Shi, and C. Lu, "Photoluminescence mechanism of carbon dots: triggering multiple color emissions through controlling the degree of protonation," *Molecules*, vol. 27, p. 6517, 2022.
- [24] S. Zhu, Y. Song, X. Zhao, J. Shao, J. Zhang, and B. Yang, "The photoluminescence mechanism in carbon dots (graphene quantum dots, carbon nanodots, and polymer dots): Current state and future perspective," *Nano Research*, vol. 8, pp. 355-381, 2015.
- [25] H. Liu, Y. Zhang, and C. Huang, "Development of nitrogen and sulfur-doped carbon dots for cellular imaging," *Journal* of *Pharmaceutical Analysis*, vol. 9, pp. 127-132, 2019.
- [26] S. R. Kamali, C.-N. Chen, D. C. Agrawal, and T.-H. Wei, "Sulfur-doped carbon dots synthesis under microwave irradiation as turn-off fluorescent sensor for Cr(III)," *Journal of Analytical Science and Technology*, vol. 12, p. 48, 2021.
- [27] S. Lu, Z. Li, X. Fu, Z. Xie, and M. Zheng, "Carbon dots-based fluorescence and UV–vis absorption dual-modal sensors for Ag<sup>+</sup> and l-cysteine detection," *Dyes and Pigments*, vol. 187 p. 109126, 2021.
- [28] H. Lu, C. Li, H. Wang, X. Wang, and S. Xu, "Biomass-derived sulfur, nitrogen co-doped carbon dots for colorimetric and fluorescent dual mode detection of silver(I) and cell imaging," *ACS Omega*, vol. 4, pp. 21500-21508, 2019.

- [29] Y. Venkatesh, P. Naidu, R. Madaraboina, and D. Kundrapu, "Synthesis of multifunctional sulfur-nitrogen co-doped carbon quantum dots via facile one-pot microwave-assisted synthesis: Applications on antioxidant, antimicrobial activities, and Fe ion sensing," *Journal of Nanoparticle Research*, vol. 27 p. 62, 2025.
- [30] H. Ding, J.-S. Wei, and H.-M. Xiong, "Nitrogen and sulfur co-doped carbon dots with strong blue luminescence," *Nanoscale*, vol. 6, pp. 13817-13823, 2014.
- [31] M. R. Hasan, N. Saha, T. Quaid, and M. T. Reza, "Formation of carbon quantum dots via hydrothermal carbonization: Investigate the effect of precursors," *Energies*, 2021.
- [32] X. Miao, X. Yan, D. Qu, D. Li, F.F. Tao, and Z. Sun, "Red emissive sulfur, nitrogen codoped carbon dots and their application in ion detection and theraonostics," ACS Applied Materials & Interfaces, vol. 9, pp. 18549-18556, 2017.
- [33] Y. Chen, Y. Wu, B. Weng, B. Wang, and C. Li, "Facile synthesis of nitrogen and sulfur co-doped carbon dots and application for Fe(III) ions detection and cell imaging," *Sensors and Actuators B: Chemical*, vol. 223, pp. 689-696, 2016.
- [34] F. Wu, M. Yang, H. Zhang, S. Zhu, X. Zhu, and K. Wang, "Facile synthesis of sulfur-doped carbon quantum dots from vitamin B1 for highly selective detection of Fe<sup>3+</sup> ion," *Optical Materials*, vol. 77, pp. 258-263, 2018.
- [35] J. Zeng, L. Liao, X. Lin, G. Liu, X. Luo, M. Luo, and F. Wu, "Red-emissive sulfur-doped carbon dots for selective and sensitive detection of mercury (II) ion and glutathione," *International Journal of Molecular Sciences*, vol. 23, p. 9213, 2022.
- [36] A. Hemmati, H. Emadi, and S. R. Nabavi, "Green synthesis of sulfur- and nitrogen-doped carbon quantum dots for determination of L-DOPA using fluorescence spectroscopy and a smartphonebased fluorimeter, ACS Omega, vol. 8, pp. 20987-20999, 2023.
- [37] A. Pal, M. P. Sk, and A. Chattopadhyay, "Recent advances in crystalline carbon dots for superior application potential," *Materials Advances*, vol. 1, pp. 525-553, 2020.
- [38] Q. Xu, P. Pu, J. Zhao, C. Dong, C. Gao, Y. Chen, J. Chen, Y. Liu, and H. Zhou, "Preparation of highly photoluminescent sulfurdoped carbon dots for Fe(III) detection," *Journal of Materials Chemistry A*, vol. 3, pp. 542-546, 2015.
- [39] X. Li, S. P. Lau, L. Tang, R. Ji, and P. Yang, "Sulphur doping: a facile approach to tune the electronic structure and optical properties of graphene quantum dots," *Nanoscale*, vol. 6 pp. 5323-5328, 2014.
- [40] N. Sahiner, S. S. Suner, M. Sahiner, and C. Silan, "Nitrogen and sulfur doped carbon dots from amino acids for potential biomedical applications," *Journal of Fluorescence*, vol. 29, pp. 1191-1200, 2019.
- [41] M. Xue, L. Zhang, Z. Zhan, M. Zou, Y. Huang, and S. Zhao, "Sulfur and nitrogen binary doped carbon dots derived from ammonium thiocyanate for selective probing doxycycline in living cells and multicolor cell imaging," *Talanta*, vol. 150 pp. 324-330, 2016.
- [42] Y.-C. Lu, J. Chen, A.-J. Wang, N. Bao, J.-J. Feng, W. Wang, and L. Shao, "Facile synthesis of oxygen and sulfur co-doped graphitic carbon nitride fluorescent quantum dots and their

- application for mercury(II) detection and bioimaging," *Journal of Materials Chemistry C*, vol. 3, pp. 73-78, 2015.
- [43] J. Yang, W. Chen, X. Liu, Y. Zhang, and Y. Bai, "Hydrothermal synthesis and photoluminescent mechanistic investigation of highly fluorescent nitrogen doped carbon dots from amino acids," *Materials Research Bulletin*, vol. 89, pp. 26-32, 2017.
- [44] W. Liu, Y. Han, M. Liu, L. Chen, and J. Xu, "Effect of defects on optical and electronic properties of graphene quantum dots: A density functional theory study," *RSC Advances*, vol. 13, pp. 16232-16240, 2023.
- [45] G. Magdy, S. Ebrahim, F. Belal, R. El-Domany, and A. A.-M. Ali, "Sulfur and nitrogen co-doped carbon quantum dots as fluorescent probes for the determination of some pharmaceuticallyimportant nitro compounds," *Scientific Reports*, vol. 13, p. 5502, 2023.
- [46] J. Jia, Y. Sun, Y. Zhang, Q. Liu, J. Cao, G. Huang, B. Xing, C. Zhang, L. Zhang, and Y. Cao, "Facile and efficient fabrication of bandgap tunable carbon quantum dots derived from anthracite and their photoluminescence properties," *Frontiers in Chemistry*, vol. 8, p. 123, 2020.
- [47] S. Kadian, G. Manik, A. Kalkal, M. Singh, and R. P. Chauhan, "Effect of sulfur doping on fluorescence and quantum yield of graphene quantum dots: An experimental and theoretical investigation," *Nanotechnology*, vol. 30, p. 435704, 2019.
- [48] Y. Wang, S.-H. Kim, and L. Feng, "Highly luminescent N, S-co-doped carbon dots and their direct use as mercury(II) sensor, Analytica Chimica Acta, vol. 890, pp. 134-142, 2015.
- [49] D. Sun, R. Ban, P.-H. Zhang, G.-H. Wu, J.-R. Zhang, and J.-J. Zhu, "Hair fiber as a precursor for synthesizing of sulfur- and nitrogen-co-doped carbon dots with tunable luminescence properties," *Carbon*, vol. 64, pp. 424-434, 2013.
- [50] N. Khadhri, M. El Khames Saad, M. ben Mosbah, and Y. Moussaoui, "Batch and continuous column adsorption of indigo carmine onto activated carbon derived from date palm petiole," *Journal of Environmental Chemical Engineering*, vol. 7 p. 102775, 2019.
- [51] Z. Zhu, P. Yang, X. Li, M. Luo, W. Zhang, M. Chen, and X. Zhou, "Green preparation of palm powder-derived carbon dots co-doped with sulfur/chlorine and their application in visible-light photocatalysis," Spectrochimica Acta Part A: Molecular and Biomolecular Spectroscopy, vol. 227, p. 117659, 2020.
- [52] G. Huang, Y. Lin, L. Zhang, Z. Yan, Y. Wang, and Y. Liu, "Synthesis of sulfur-selenium doped carbon quantum dots for biological imaging and scavenging reactive oxygen species, *Scientific Reports*, vol. 9, p. 19651, 2019.
- [53] S. Sun, Q. Guan, Y. Liu, B. Wei, Y. Yang, and Z. Yu, "Highly luminescence manganese doped carbon dots," *Chinese Chemical Letters*, vol. 30, pp. 1051-1054, 2019.
- [54] J. P. Paraknowitsch, Y. Zhang, B. Wienert, and A. "Thomas, nitrogen- and phosphorus-co-doped carbons with tunable enhanced surface areas promoted by the doping additives," *Chemical Communications*, vol. 49, pp. 1208-1210, 2013.
- [55] T. Zhang, Q. Ji, J. Song, H. Li, X. Wang, H. Shi, M. Niu, T. Chu, F. Zhang, and Y. Guo, "Preparation of nitrogen and sulfur codoped fluorescent carbon dots from cellulose nanocrystals as

- a sensor for the detection of rutin," *Molecules*, vol. 27, p. 8021, 2022.
- [56] K. Nguyen, I.-A. Baragau, R. Gromicova, A. Nicolaev, S. Thomson, A. Rennie, N. Power, M. Sajjad, and S. Kellici, "Investigating the effect of N-doping on carbon quantum dots structure, optical properties and metal ion screening," *Scientific Reports*, vol. 12, p. 13806, 2022.
- [57] B. Wang, Y. Wang, Y. Zhou, F. Qi, Q. Ding, J. Li, X. OuYang, and L. Liu, "Multi-walled carbon nanotube-reinforced boron carbide matrix composites fabricated via ultra-high-pressure sintering," *Journal of Materials Science*, vol. 54, pp. 11084-11095, 2019.
- [58] R. S. Vartapetyan, A. M. Voloshchuk, and E. B. Shumilina, "The critical size of clusters of water molecules on a carbon surface," *Russian Chemical Bulletin*, vol. 42, pp. 46-48, 1993.
- [59] H. Hantsche, "High resolution XPS of organic polymers, the scienta ESCA300 database," *Journal of Chemical Education*, vol. 70, no. 1, 1993.
- [60] X. Chen, and J. Che, "Nitrogen and sulfur co-doped carbon dots derived from granatums and ammonium persulfate to detect tetracyclines in milk," *Food Chemistry Advances*, vol. 1 p. 100112, 2022.
- [61] M. Hamid, S. Humaidi, H. Wijoyo, I. Isnaeni, I. R. Saragi, C. Simanjuntak, N. H. M. Kaus, M. M. A. Kechik, A. Nurbillah, Y. Yaakob, and T. I. Nasution, "Solvothermal synthesized N–S doped carbon dots derived from cavendish banana peel (Musa paradisiaca) for detection of Fe(III) and Pb(II)," *Chemical and Environmental Engineering*, vol. 10, p. 100832, 2024.
- [62] Y. Wu, Y. Li, J. Gao, and Q. Zhang, "Recent advances in vacancy engineering of metal-organic frameworks and their derivatives for electrocatalysis," *SusMat*, vol. 1, pp. 66-87, 2021.
- [63] S. Jamil, R. Afzal, S. R. Khan, M. Shabbir, N. Alhokbany, S. Li, and M. R. S. A. Janjua, "Photocatalytic degradation of indigo carmine dye by hydrothermally synthesized graphene nanodots (GNDs): Investigation of kinetics and thermodynamics," RSC Advances, vol. 14, pp. 23973-23986, 2024.
- [64] Y. Zhou, E. M. Zahran, B. A. Quiroga, J. Perez, K. J. Mintz, Z. Peng, P. Y. Liyanage, R. R. Pandey, C. C. Chusuei, and R. M. Leblanc, "Size-dependent photocatalytic activity of carbon dots with surface-state determined photoluminescence," *Applied Catalysis B: Environmental*, vol. 248, pp. 157-166, 2019.
- [65] P. Hao, R. Shi, X. Wang, J. Zhang, B. Li, J. Wang, B. Liu, Y. Liu, X. Qiao, and Z. Wang, "Efficient tetracycline degradation using carbon quantum dot modified TiO<sub>2</sub>@LaFeO<sub>3</sub> hollow core shell photocatalysts," *Scientific Reports*, vol. 14, p. 27057, 2024.
- [66] M. A. Adib, F. Sharmin, and M. A. Basith, "Tuning the morphology, stability and optical properties of CsSnBr<sub>3</sub> nano-crystals through bismuth doping for visible-light-driven applications," *Nanoscale Advances*, vol. 5, pp. 6194-6209, 2023.
- [67] *Mulliken Electronegativity*, 1966, Nobel Prize in Chemistry pp. 1896–1986,
- [68] P. Cheng, Z. Yang, H. Wang, W. Cheng, M. Chen, and W. Shangguan, "TiO<sub>2</sub>-graphene nanocomposites for photocatalytic hydrogen production from splitting water," *Fuel and Energy Abstracts*, vol. 37, pp. 2224-2230, 2012.

- [69] V. Takhar, and S. Singh, "Nanomaterials ROS: A comprehensive review for environmental applications," *Environmental Science: Nano*, vol. 12, pp. 2516-2550, 2025.
- [70] S. San Martín, M.J. Rivero, and I. Ortiz, "Unravelling the mechanisms that drive the performance of photocatalytic hydrogen production," *Catalysts*, vol. 10, p. 901, 2020.